Structural peculiarities, point defects and luminescence in Bi-doped CsCdX_3 (X = Cl, Br) single crystals

Daria N. Vtyurina [a], Irina A. Kaurova [b, *], Galina M. Kuz'micheva [b], Victor B. Rybakov [c], Dmitry Yu. Chernyshov [d], Evgeny V. Khramov [e], Sergey V. Firstov [f], Vladimir N. Korchak [a]

[a] Semenov Institute of Chemical Physics, Russian Academy of Sciences, 4-1 Kosygina str, Moscow, 119991, Russia
[b] MIREA - Russian Technological University, 78 Vernadskogo pr, Moscow, 119454, Russia
[c] Lomonosov Moscow State University, 1-3 Vorobyovy Gory, Moscow, 119992, Russia
[d] Swiss-Norwegian Beamlines at the European Synchrotron Radiation Facility, 38000, Grenoble, France
[e] National Research Center "Kurchatov Institute", 1 Akademika Kurchatova pl, Moscow, 123182, Russia
[f] Fiber Optics Research Center, Russian Academy of Sciences, 38 Vavilov str, Moscow, 119333, Russia

ARTICLE INFO

ABSTRACT

Promising luminescent CsCdX_3 (X = Cl, Br) single crystals, both nominally-pure and doped with bismuth, have been studied comprehensively by X-ray diffraction, X-ray synchrotron radiation, and X-ray absorption spectroscopy. Crystal structure refinement shows vacancies in the Cs crystallographic site and partial substitution of Cd^{2+} ions by Bi^{3+} ones in both CsCdCl$_3$ and CsCdBr$_3$ (point defects Bi$^\bullet_{Cd}$), which is consistent with the results of X-ray absorption spectroscopy. The assumed presence of Bi^{1+} ions in the Cs^{1+} sites of doped CsCdX_3 (X = Cl, Br) crystals is not confirmed. In the photoluminescence spectra of Bi-doped CsCdCl$_3$ and CsCdBr$_3$ crystals, a single band in the near-IR spectral range with a maximum around 1000 nm is caused by point defects Bi$^\bullet_{Cd}$. Photoluminescence spectra and decay kinetics of Bi-doped CsCdX_3 (X = Cl, Br) indicate their promising use as luminescent materials.

1. Introduction

Luminescent materials with high photoluminescence (**PL**) efficiency in the near-IR spectral range (900−1600 nm) are useful in a variety of applications, in particular, in photonics, medicine, and metrology. These include halides doped with the Bi^{1+} ions, which are promising materials for new tunable lasers and optical amplifiers [1−3]. In addition, halide crystals are transparent in a wide spectral range and possess high resistance to optical damage.

Although some spectral characteristics of bismuth centers in several crystalline compounds are known [4,5] and optical properties of Bi-doped halides are partially studied [6−8], a location of the Bi^{1+} cation in these crystal matrices has not yet been precisely defined as well as its formal charge has not been confirmed (Table 1). Only Vtyurina et al. [8], according to X-ray diffraction and X-ray absorption spectroscopy, revealed a presence of Bi^{1+} ions,

which can occupy interstitial (Bi$^\bullet_i$) and Tl (Bi$^\times_{Tl}$) sites and only interstitial (Bi$^\bullet_i$) sites in the structures of Bi-doped TlCdCl$_3$ and TlCdI$_3$ crystals, respectively. In addition, a correlation between optical centers and point defects in the structures of the above-mentioned crystals was determined [8], which makes it possible to perform a controlled synthesis of both these and new optically active media.

With regards to the CsCdX_3 (X = Cl, Br) crystals, it was only suggested that the Bi^{1+} ions can isomorphically substitute the Cs^{1+} ions in the CsCdCl$_3$ crystal matrix due to their similar ionic radii [9]. Wolfert and Blasse suggested that the Bi^{3+} ions are incorporated into the CsCdBr$_3$ and CsMgCl$_3$ lattices [10]. However, any experimental evidence of both structural location and formal charge of Bi cations in the CsCdX_3 (X = Cl, Br) structures is absent in the literature. The present study was undertaken to clarify this point.

2. Material and methods

To obtain Bi-doped CsCdCl$_3$ (**CsCdCl$_3$:Bi**) and CsCdBr$_3$ (**CsCdBr$_3$:Bi**) single crystals, double chlorides and bromides taken

Table 1
Luminescent parameters and optical centers in several complex halides.

Crystal	PL band maximum, nm	Characteristic PL decay time, μs	Optical centers
KMgCl$_3$:Bi [1]	950	400	$(Bi_K)^{\times a}$
KAlCl$_4$:Bi [1]	980	525	
RbPb$_2$Cl$_5$:Bi [4]	1080	140	$(Bi_{Rb})^{\times a}$
TlCdCl$_3$:Bi^{1+} [8]	1025	150 and 170	$(Bi_{Tl})^{\times b}$
	1253		$Bi_i^{\bullet b}$
TlCdI$_3$:Bi^{1+} [8]	1175	30 and 35	$Bi_i^{\bullet b}$
CsCdCl$_3$:Bi^{3+} (present work)	980	540	$Bi_{Cd}^{\bullet b}$
CsCdBr$_3$:Bi^{3+} (present work)	1056	260	$Bi_{Cd}^{\bullet b}$

a it was assumed based on the close ionic radii.
b it was found by X-ray diffraction and/or EXAFS/XANES measurements.

in a molar ratio of CdCl$_2$: CsCl : BiCl$_3$ = 59.8 : 39.8 : 0.4 and CdBr$_2$: CsBr : BiBr$_3$ = 54.5 : 44.5 : 1, respectively, were used. A metallic bismuth was added in a molar ratio of Bi$_{Me}$/BiCl$_3$ = 0.03 and Bi$_{Me}$/BiBr$_3$ = 1, assuming a formation of Bi^{1+} ions. Due to the hygroscopic nature of reagents, all the procedures such as weighing and mixing of components and their placing into a quartz ampoule were carried out in an argon-filled Labconco glove box. The filled ampoule was removed from the box, pumped out to the forevacuum, blown with helium, re-pumped out and then sealed off at the preformed waist.

The nominally-pure CsCdBr$_3$ and Bi-doped CsCdBr$_3$ and CsCdCl$_3$ single crystals were grown by the Bridgman-Stockbarger technique at an ampule lowering rate of 2 mm h^{-1}. The temperatures in the upper and lower zones of the furnace were, respectively, 580 and 530 °C for the CsCdCl$_3$:Bi and 450 and 380 °C for the CsCdBr$_3$:Bi. After completion of the growth process, the crystals were cooled to room temperature at a rate of 0.33 °C min^{-1}.

The as-grown CsCdCl$_3$:Bi crystal had a pale green-blue color (Fig. 1a) and consisted of many single crystals a few millimeters in size. Polycrystalline boule could be formed due to the non-stoichiometric composition of the melt or due to the presence of BiCl$_3$ in the initial batch. The largest individual single crystals taken from the lower part of the boule were selected for the investigation; optically-transparent samples with surfaces parallel to the main optical axis of the crystal (the 6-fold axis) were fabricated. According to the energy-dispersive X-ray microanalysis (FEI Quanta 200 3D), the Cd, Cs, and Cl content in the CsCdCl$_3$:Bi crystal is 20.67, 20.20, 59.95 at.%, respectively. According to the inductively coupled plasma mass spectrometry (**ICP-MS**) data (Thermo Scientific iCAP Q ICP-MS), the content of bismuth in the CsCdCl$_3$:Bi is 0.4 at.%.

The as-grown CsCdBr$_3$:Bi crystal had a yellow-green color (Fig. 1b) and consisted of a polycrystalline mass at the top and a significant single-crystal part at the conical base. Single-crystal samples were separated from the boule and then polished. The largest individual single crystals were selected for the investigation. According to the energy-dispersive X-ray microanalysis (FEI Quanta

200 3D), the Cd, Cs, and Br content in the CsCdBr$_3$:Bi and CsCdBr$_3$ crystals is 19.92, 16.85, 63.23 and 20.35, 20.91, 58.74, respectively. According to the ICP-MS data (Thermo Scientific iCAP Q ICP-MS), the content of bismuth in the CsCdBr$_3$:Bi is 0.8 at.%.

The X-ray diffraction (**D**) analysis of the CsCdBr$_3$, CsCdBr$_3$:Bi, and CsCdCl$_3$:Bi microcrystals ∼ 0.1 × 0.1 × 0.1 mm^3 in size was performed with an Enraf-Nonius CAD-4 single-crystal diffractometer at room temperature (AgK$_\alpha$, graphite monochromator, ω - scan mode). To reduce an error associated with absorption, the X-ray diffraction data were collected over the entire Ewald sphere. The preliminary data processing was carried out using the WinGX pack [11].

The CsCdBr$_3$, CsCdBr$_3$:Bi, and CsCdCl$_3$:Bi crystals were studied using X-ray synchrotron radiation (**S**) on a Swiss-Norwegian Beamlines (**SNBL**) at the European Synchrotron Radiation Facility, Grenoble, France at room temperature (λ = 0.69990 Å). The single-crystal data were preprocessed with the SNBL Tool Box [12], the integral intensities were extracted from frames with the CrysAlisPro software [13].

Crystal structures were refined with the SHELXL-14 [14]. The atomic coordinates, atom displacement parameters of all atoms, and occupancies of cation and oxygen sites were refined using the SHELXL-14 software package [14], taking into account atomic scattering curves for neutral atoms, with a semi-empirical (azimuthal scan) correction of absorption [15].

The structural parameters were refined in several steps. Initially, the positional and displacement parameters were simultaneously refined in isotropic and anisotropic approximations. Then the refinement of displacement parameters together with occupancy of Cs site was performed with fixed occupancies of Cd and Cl/Br sites. Then the refinement of occupancy of Cd site was carried out with fixed occupancy of Cl/Br site, and, finally, occupancy of Cl/Br site was refined with fixed occupancy of Cd site. Due to the well-known correlation between displacement parameters and site occupancies we used the strategy of crystal structure refinement developed by us for both present objects and other complex oxides and described in detail [8,16]. After each refinement step, the residual electron density, displacement parameters, and interatomic distances were analyzed. The real compositions taking into account the electro-neutrality, the correct values of the displacement parameters, the lowest values of the R factors, and the absence of residual electron-density peaks serve as criteria for the accuracy of the structure refinement and the correctness of the determination of compositions.

X-ray absorption spectroscopy (**EXAFS/XANES**) measurements (∼100 mg) were performed at room temperature at the Structural Materials Science end-station at the Kurchatov synchrotron radiation source [17]. Samples (∼100 mg) were ground to a powder and evenly applied on the adhesive tape, having small X-ray absorption coefficient. The energy scans were performed using Si(220)-crystal monochromator with the energy resolution ΔE/E ∼ 2·10^{-4}. The

5 mm   *a*   1 cm   *b*
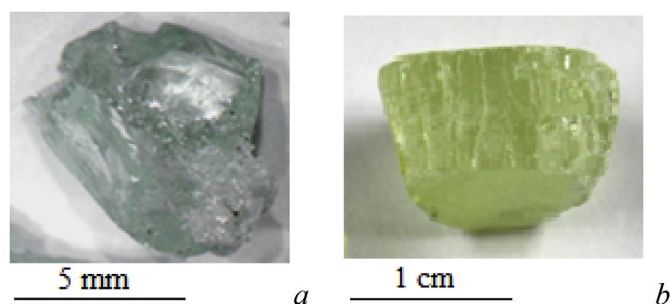
Fig. 1. Photos of Bi-doped CsCdCl$_3$ (*a*) and CsCdBr$_3$ (*b*) single crystals.

XAFS spectra were collected at the Cs and Cd K edges in a transmission mode, placing the sample between two ionization chambers connected to picoammeter (Keithley), which also serves as a voltage source. The intensity of the monochromatic beam, incident on the sample and passing through it, was measured in air ionization chamber and chamber filled with pure Ar up to atmospheric pressure, respectively.

A standard processing of experimental spectra was performed using IFEFFIT program package [18]. A character of the atom's immediate environment was revealed by analyzing a radial distribution function $\varphi(r)$ obtained by Fourier transform of $k^3 \cdot \chi(k)$ function during the experiment, where the multiplication by k^3 was used to compensate attenuation of Fourier transforms with distance from the absorption edge. Fourier transforms of EXAFS oscillations were extracted in the range of photoelectron wave number (k) from 2 to 12.0 Å^{-1} at the both edges and modeled in the range of interatomic distance (d_{EXAFS}, Å) from 1.0 to 3.5 Å at the Cs edge, and from 1.0 to 3.2 Å at the Cd edge.

Photoluminescence (**PL**) spectra for the Bi-doped CsCdBr$_3$ sample were studied on an SDH-IV spectrometer (Solar Laser Systems, Belarus) in the range of 880—1700 nm at $T = 77$ and 300 K. An Osram HBO 150W xenon lamp combined with LOMO MDR-12 monochromator was used as a variable wavelength light source. PL spectra for the Bi-doped CsCdCl$_3$ crystal are published in Ref. [19].

Photoluminescence decay kinetics for Bi-doped CsCdCl$_3$ and CsCdBr$_3$ samples was studied with an Edinburgh Instruments FLS920 spectrofluorimeter equipped with a 450 W xenon lamp.

3. Results and discussion

3.1. Crystal structure studies

The CsCdBr$_3$ (**CCB**) and CsCdCl$_3$ (**CCC**) compounds belong to the perovskite family (space group $Pm3m$, $Z = 1$; $a_0 \sim 2(r_{Cd}^{VI} + R_X)$ Å or $a_0 \sim \sqrt{2}(r_{Cs}^{XII} + R_X)$ Å, where r_{Cd}^{VI}, r_{Cs}^{XII}, and R_X are ionic radii for the Cd^{2+}, Cs^{1+}, and $X =$ Br, Cl [20] depending on the coordination number (**CN**)) and crystallize in the space group $P6_3/mmc$ with the unit cell parameters $a = 7.675(3)$ Å ($a \sim a_0\sqrt{2}$), $c = 6.722(3)$ Å ($c_0 \sim 2/3a_0\sqrt{3}$) and $a = 7.418(4)$ Å ($a \sim a_0\sqrt{2}$), $c = 18.39(3)$ Å ($c_0 \sim 2a_0\sqrt{3}$), respectively [21,22]. In the CsCdBr$_3$ (Fig. 2) and CsCdCl$_3$ (Fig. 3) crystal structures, Cd atoms are located in octahedra (CNCd = 6) and Cs atoms occupy hexagonal cuboctahedra (CNCs = 12).

An initial CaTiO$_3$ perovskite structure can be described as a cubic packing (c-packing) of trigonal CaO$_3$ layers with the Ti^{4+} ions in octahedral voids. The CsCdBr$_3$ (CsNiCl$_3$-type structure) and CsCdCl$_3$ (CsMgF$_3$-type structure) crystal structures can be described, respectively, as a two-layer hexagonal packing (h-packing) of the CsBr$_3$ trigonal layers (Fig. 2b) and a mixed six-layer hexagonal packing (hcc-package) of the CsCl$_3$ trigonal layers (Fig. 3b), in which octahedral voids are occupied by the Cd^{2+} ions [23].

The radii of the Cs^{1+} and Bi^{1+} as well as Cd^{2+} and Bi^{3+} ions are similar, hence, a substitution of the Cs^{1+} ions ($r_{Cs}^{XII} = 1.88$ Å) by the Bi^{1+} ones ($r_{Bi}^{XII} = 1.903$ Å) ($\Delta_r = 0.023$ Å) or the Cd^{2+} ions ($r_{Cd}^{VI} = 0.95$ Å) by the Bi^{3+} ones ($r_{Bi}^{VI} = 1.03$ Å) ($\Delta_r = 0.08$ Å) is possible. According to the isomorphism theory [24], in addition to the atomic sizes, electronegativity values (χ) of the components should also be taken into account. Hence, the Bi^{3+} ions are most likely to substitute for the Cd^{2+} ones ($\chi_{Cs1+} = 0.7$ a.u. and $\chi_{Bi1+} = 1.4$ a.u., $\Delta_\chi = 0.7$ a.u.; $\chi_{Cd2+} = 1.5$ a.u. and $\chi_{Bi3+} = 1.8$ a.u., $\Delta_\chi = 0.3$ a.u.).

A refinement of the CsCdBr$_3$ crystal structure based on the X-ray diffraction (**D**) and synchrotron (**S**) data (Tables 2 and 3) resulted in the compositions CsCdBr$_{2.976(42)}$ (almost stoichiometric composition taking into account the standard deviation) and CsCdBr$_3$ (stoichiometric composition) (Table 4), respectively. A crystal structure of CsCdBr$_3$ consists of linear chains formed by the CdBr$_6$ octahedra with six equal Cd−6Br interatomic distances, elongated along the c axis and interconnected by the Cs^{1+} ions (Fig. 2c, Table 3). The distance between two Cd^{2+} ions in the chain (3.360(1) Å (D) and 3.3822(1) Å (S)) is less than half of that between the chains (~7.6 Å), i.e. the structure is quasi-one-dimensional. In a hexagonal cuboctahedron, there are two types of distances CNCs = 6Br + 6Br (Table 3, Fig. 2a).

A refinement of site occupancy in the CsCdBr$_3$:Bi(D) structure revealed a decrease and an increase in the occupancy of Cs and Cd sites, which indicates a deficiency of the Cs site (V$_{Cs}$'; V - vacancies) and a presence of the Bi^{3+} ions in the Cd site (Bi$_{Cd}$•), since a site occupancy is proportional to atomic number of the element (N(Cs) = 55, N(Cd) = 43, N(Bi) = 83). Hence, a composition of the CsCdBr$_3$:Bi(D) micropart can be written as (Cs$_{0.990(1)}$□$_{0.010}$)(Cd$_{0.991(2)}$Bi$^{3+}_{0.009}$)Br$_{2.970(30)}$ (- vacancies) ($0 \rightarrow$ V$_{Cs}$' + Bi$_{Cd}^{•}$, Equation (1)). A similar refined composition was obtained for the micropart taken from another region of the as-grown CsCdBr$_3$:Bi crystal: (Cs$_{0.976(10)}$□$_{0.024}$)(Cd$_{0.967(47)}$Bi$^{3+}_{0.033}$)Br$_3$ (Eq. (1) is applied) (CsCdBr$_3$:Bi(S)) (Table 4). If the standard deviation of the Br site occupancy value in the refined composition of the CsCdBr$_3$:Bi(D) sample is not taken into account, the vacancies in the Br site (V$_{Br}^{•}$) can be added: (Cs$_{0.990(1)}$□$_{0.010}$)(Cd$_{0.991(2)}$Bi$^{3+}_{0.009}$)(Br$_{2.970(30)}$□$_{0.030}$) ($0 \rightarrow 2$V$_{Cs}$' + Bi$_{Cd}^{•}$ + V$_{Br}^{•}$, Equation (2)).
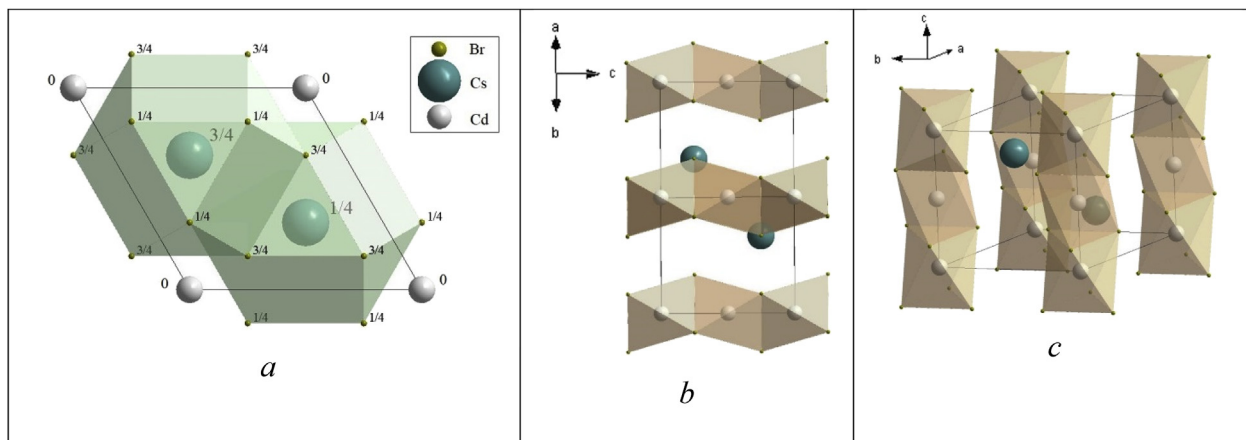

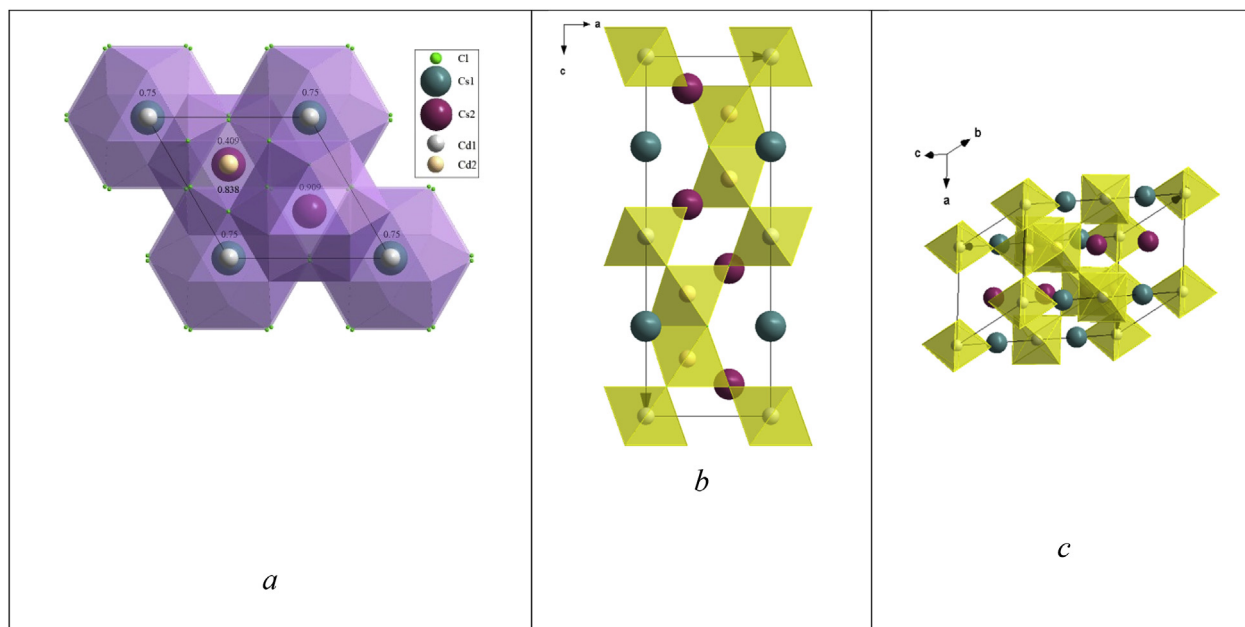**Fig. 2.** Crystal structure of the CsCdBr$_3$ with polyhedra for the Cs (a) and Cd (b,c) atoms.

Fig. 3. Crystal structure of the CsCdCl$_3$ with polyhedra for the Cs (a) and Cd (b,c) atoms.

It should be noted that in the structures of CsCdBr$_3$ crystals doped with the Pr^{3+} [25] ($r_{Pr}^{VI} = 0.99$ Å), Ho^{3+} [26] ($r_{Ho}^{VI} = 0.90$ Å), Tm^{3+} ($r_{Tm}^{VI} = 0.88$ Å) [27], and Yb^{3+} ($r_{Yb}^{VI} = 0.87$ Å) [28] ions, a substitution of the Cd^{2+} ($r_{Cd}^{VI} = 0.95$ Å) cations located in quasi-one-dimensional linear chains for rare-earth ions (Ln^{3+}) was established by electron paramagnetic resonance and selective excitation and fluorescence spectroscopy studies. In this case, dimers ($Ln^{3+} - V_{Cd}'' - Ln^{3+}$) are formed in the chain, the total electric charge of which is equal to that of three substituted Cd^{2+} ions. This type of substitution preserves an electroneutrality of crystal without any participation of additional charge compensators. A formation of asymmetric dimers, in which two Ln^{3+} ions substitute for the neighboring Cd^{2+} ions and the Cd^{2+} vacancy (V_{Cd}'') is located close to one of the Ln^{3+} ions, is also possible [26]. A comparison of energies of lower excited electronic levels measured for the isolated ion and symmetric dimer with the data obtained for a similar sample using laser selective excitation spectroscopy allowed to uniquely identify optical spectra and conclude that the center responsible for an up-conversion luminescence in the CsCdBr$_3$:Tm^{3+} crystals is the symmetric dimer Tm$^{3+} - V_{Cd}'' - Tm^{3+}$ ($0 \rightarrow V_{Cd}'' + 2Tm_{Cd}^\bullet$; Equation (3)) [27]. It follows that the structural behavior of Ln^{3+} and Bi^{3+} ions in the CsCdBr$_3$ crystal matrix is similar.

Fig. 4 shows the unit cell parameters of un-doped and Bi-doped CsCdX_3 crystals depending on the type of X anion ($X =$ Cl, Br). It can be seen that the a and c unit cell parameters are varied antibatically with increasing (decreasing) radius of the X anion. The unit cell parameters of CsCdBr$_3$ (D and S) crystals are larger than those of CsCdBr$_3$:Bi (D and S) ones (Fig. 4), the Cs−Br interatomic distances in the CsCdBr$_3$ (D) structure being larger than those in the CsCdBr$_3$:Bi (D) one (Table 3). This behavior of the structural parameters supports Eq. (2), i.e. there are vacancies in the Br site ($V_{Br}^\bullet$), which in most cases reduces the unit cell parameters.

The crystal structure of CsCdCl$_3$ differs from that of CsCdBr$_3$: the atomic sites are doubled in the CsCdCl$_3$ unit cell compared to the CsCdBr$_3$ one (Fig. 3). A refinement of site occupancy in the CsCdCl$_3$:Bi(D) structure showed only vacancies in the Cs1 site and a partial substitution of the Cd^{2+} ions by the Bi^{3+} ones in both Cd crystallographic sites: (Cs1$_{0.989(1)}\square_{0.011}$)Cs2(Cd1$_{0.995(2)}Bi^{3+}_{0.005}$)

(Cd2$_{0.996(2)}$Bi$^{3+}_{0.004}$)Cl$_6 \equiv$ (Cs$_{0.995(2)}\square_{0.005}$)(Cd$_{0.996(2)}Bi^{3+}_{0.004}$)Cl$_3$ (Eq. (1) is applied) (Tables 3 and 4).

In the structure of CsCdCl$_3$:Bi(S) crystal determined at 200 K, the occupancies of Cs1 and Cs2 sites decrease and those of Cd1 and Cd2 sites increase, and the Cl sites are defect-free (Table 3). The refined composition of the CsCdCl$_3$:Bi(S) sample can be written as (Cs1$_{0.9948(2)}\square_{0.0052}$)(Cs2$_{0.9985(2)}\square_{0.0015}$)(Cd1$_{0.9873(7)}Bi^{3+}_{0.0127}$) (Cd2$_{0.9972(43)}Bi^{3+}_{0.0028}$)Cl$_6 \equiv$ (Cs$_{0.9966(2)}\square_{0.0034}$)(Cd$_{0.9923(25)}Bi^{3+}_{0.0077}$) Cl$_3$ (Eq. (1) is applied) (Tables 3 and 4). It does not contradict the refined composition of the CsCdCl$_3$:Bi(D) sample. A clear correlation between the Bi^{3+} content in the CsCdX_3:Bi and a type of the X ion is observed: for the $X =$ Br ($R_{Br} > R_{Cl}$), the concentration of Bi^{3+} ions in the crystal structure is higher (Table 4), which is confirmed by the ICP-MS data. This is consistent with the theory of isomorphic mixing of components [24], in particular, with the rule of assistance: an increase in the size of structural unit (in our case, the X size) expands the mixing ability (in our case, the Bi$_{Cd}^\bullet$ content is greater in the CsCdBr$_3$:Bi; $R_{Br} > R_{Cl}$). Moreover, a small degree of isomorphic substitution of Cd^{2+} ions by the Bi^{3+} ones (Bi$_{Cd}^\bullet$) is due to another rule of isomorphism, namely, the rule of polarity: cations with larger radii (in our case, the Bi^{3+} cations) are more difficult to enter into the crystal lattice composed of cations having lower radii (in our case, the Cd^{2+} cations; $r_{Bi} > r_{Cd}$) and vice versa.

Therefore, a presence of Bi^{1+} ions in the crystals under investigation was not found by X-ray diffraction analysis.

3.2. X-ray absorption spectroscopy studies

The XANES spectra measured at the Cd K-edge for the CsCdBr$_3$ and CsCdBr$_3$:Bi samples are identical (Fig. 5a). The XANES spectrum for the CsCdCl$_3$:Bi has a similar structure near the absorption edge, while more distant oscillations differ due to a different local atomic structures of chloride and bromide.

The EXAFS technique is element-specific; however, it is not able to distinguish atoms of one element having different coordination. Atoms of one element being located in different phases or in different crystallographic sites in one phase, the EXAFS data represents an average picture for all types of coordination environment. The EXAFS fitting for these atoms requires normalization of

Table 2
Crystallographic data, experimental details and structure refinement statistics for undoped and Bi-doped $CsCdX_3$ (X = Cl, Br) crystals according to the X-ray diffraction (**D**) and X-ray synchrotron radiation (**S**) data.

Nominal composition	CsCdBr$_3$		CsCdBr$_3$:Bi		CsCdCl$_3$:Bi	
Technique	D	S	D	S	D	S
Sample abbreviation	CCB(D)	CCB(S)	CCB:Bi(D)	CCB:Bi(S)	CCC:Bi(D)	CCC:Bi(S)
System, Space group	Hexagonal, $P6_3/mmc$					
Z			2		6	
a, Å	7.762(4)	7.7167(2)	7.669(3)	7.7119(3)	7.397(1)	7.3608(2)
c, Å	6.719(3)	6.7644(3)	6.715(2)	6.7605(2)	18.406(7)	18.3243(5)
V, Å^3	350.57	348.84	341.98	348.20	872.08	859.82
D_x, g cm^{-3}	4.595	4.618	5.725	4.740	4.416	4.151
Radiation λ, Å	Enraf-Nonius CAD-4, Ag$K\alpha$, 0.55941	Synchrotron, 0.69990	Enraf-Nonius CAD-4, Ag$K\alpha$, 0.55941	Synchrotron, 0.69990	Enraf-Nonius CAD-4, Ag$K\alpha$, 0.55941	Synchrotron, 0.69990
Absorption μ, mm^{-1}	13.42	25.32	20.78	63.31	8.60	16.39
T, K	295					200
Sample size, mm	~0.1 × 0.1 × 0.1	>0.1 × 0.1 × 0.1	~0.1 × 0.1 × 0.1	>0.1 × 0.1 × 0.1	~0.1 × 0.1 × 0.1	>0.1 × 0.1 × 0.1
Type of scan	Ω					
$2\theta_{max}$, deg	49.46	49.79	49.80	50.44	43.81	50.82
Limits h, k, l	$-11 \leq h \leq 11$, $-11 \leq k \leq 11$, $-10 \leq l \leq 10$	$-7 \leq h \leq 7$, $-9 \leq k \leq 9$, $-7 \leq l \leq 7$	$-11 \leq h \leq 11$, $-11 \leq k \leq 11$, $-10 \leq l \leq 10$	$-8 \leq h \leq 8$, $-6 \leq k \leq 6$, $-7 \leq l \leq 7$	$-9 \leq h \leq 9$, $-9 \leq k \leq 9$, $-24 \leq l \leq 24$	$-8 \leq h \leq 8$, $-6 \leq k \leq 6$, $-21 \leq l \leq 21$
No. of reflections: measured/unique ($I > 2\sigma(I)$)	4941/266	1100/141	4907/265	1353/141	8652/461	3243/347
No. of parameters in refinement	10	9	10	9	26	24
Weighting scheme	$1/[\sigma^2(F_0^2) + (0.0570P)^2 + 7.30P]$	$1/[\sigma^2(F_0^2) + (0.1184P)^2 + 6.17P]$	$1/[\sigma^2(F_0^2) + (0.0379P)^2 + 16.01P]$	$1/[\sigma^2(F_0^2) + (0.1409P)^2 + 4.11P]$	$1/[\sigma^2(F_0^2) + (0.0165P)^2 + 4.72P]$	$1/[\sigma^2(F_0^2) + (0.1446P)^2]$
	$P = (F_0^2 + 2F_c^2)/3$					
R_1 ($I > 2\sigma(I)$) wR_2	0.0687	0.0589	0.0391	0.0690	0.0287	0.0680
S	0.1625	0.1799	0.1073	0.0705	0.0608	0.2083
	1.115	1.215	1.164	1.311	1.373	1.081

Table 3
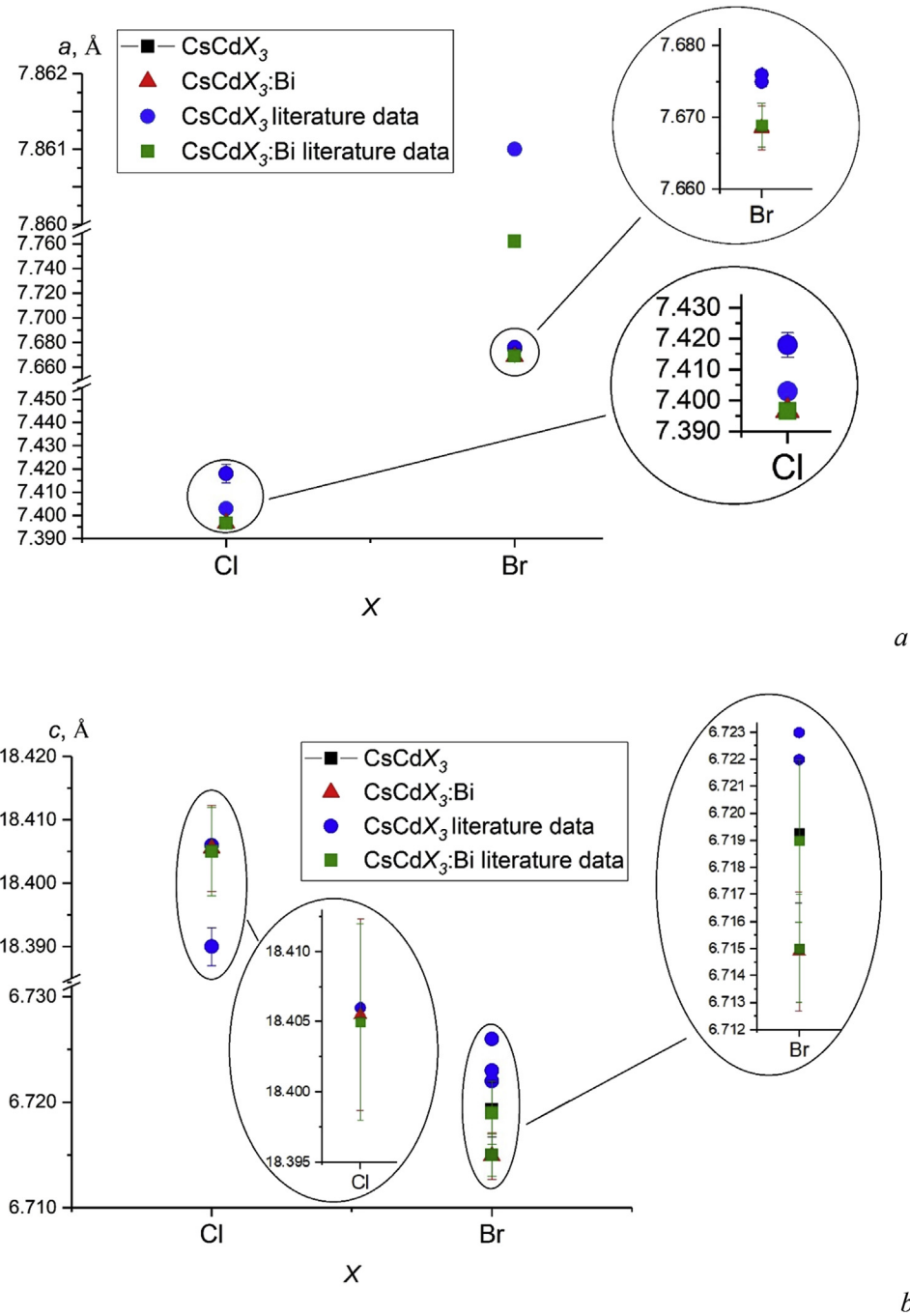
Coordinates of atoms and their equivalent thermal parameters $B_{eq} \times 10^2$ (Å^2), site occupancies p (SOF) and main interatomic distances d (Å) in the structures of undoped and Bi-doped CsCdX_3 (X = Cl, Br) crystals according to the X-ray diffraction (**D**) and X-ray synchrotron radiation (**S**) data.

Nominal composition	CsCdBr$_3$		CsCdBr$_3$:Bi		CsCdCl$_3$:Bi	
Technique	D	S	D	S	D	S
Sample abbreviation	CCB(D)	CCB(S)	CCB:Bi(D)	CCB:Bi(S)	CCC:Bi(D)	CCC:Bi(S)
Cs/Cs1						
x	2/3	2/3	2/3	2/3	0	0
y	1/3	1/3	1/3	1/3	0	0
z	1/4	1/4	1/4	1/4	1/4	1/4
p	0.16667	0.16667	0.1650(2)	0.1627(2)	0.1648(2)	0.16575(3)
B_{eq}	4.63(8)	4.2(1)	4.608(2)	3.3(2)	2.82(4)	5.4(1)
Cs2						
x					1/3	1/3
y					2/3	2/3
z					0.08888(4)	0.08826(5)
p					0.16667	0.16642(3)
B_{eq}					2.88(4)	5.5(1)
Bi/Bi1						
x			0	0	0	0
y			0	0	0	0
z			0	0	0.089(4)	0
p			0.0015(3)	0.006(8)	0.0008(3)	0.00212(12)
B_{eq}			3.005(1)	2.4(2)	2.82(4)	4.8(1)
Bi2						
x					1/3	1/3
y					2/3	2/3
z					0.08888(4)	0.83989(5)
p					0.00067(28)	0.00047(12)
B_{eq}					2.88(4)	4.8(1)
Cd/Cd1						
x	0	0	0	0	0	0
y	0	0	0	0	0	0
z	0	0	0	0	0	0
p	0.16667	0.16667	0.1652(3)	0.161(8)	0.1658(3)	0.16455(12)
B_{eq}	3.03(6)	3.2(1)	3.005(1)	2.4(2)	1.48(3)	4.8(1)
Cd2						
x					1/3	1/3
y					2/3	2/3
z					0.84039(3)	0.83989(5)
p					0.1660(3)	0.16620(12)
B_{eq}					1.38(3)	4.8(1)
Br/Cl1						
x	1/6	1/6	1/6	1/6	0.1658(1)	0.16578(7)
y	1/3	1/3	1/3	1/3	0.8342(1)	0.83422(7)
z	1/4	1/4	1/4	1/4	0.91851(8)	0.9184(1)
p	0.496(7)	0.5000	0.495(5)	0.5000	0.5000	0.5000
B_{eq}	3.31(8)	4.4(1)	3.348(1)	2.6(2)	2.99(4)	5.7(1)
Cl2						
x					0.4932(2)	0.4938(2)
y					0.5068(2)	0.5062(1)
z					3/4	3/4
p					0.2500	0.2500
B_{eq}					1.93(5)	5.1(1)
Cs − 6 × Br	3.881(2)	3.8583(1)	3.834(2)	3.8559(1)		
− 6 × Br	4.038(1)	4.0499(1)	4.022(1)	4.0475(1)		
[Cs−Br]$_{avr}$	3.9595	3.9541	3.928	3.9517		
Cs1 − 6 × Cl2					3.6994(5)	3.6813(1)
− 6 × Cl1					3.759(2)	3.740(2)
[Cs1−Cl]$_{avr}$					3.7292	3.71065
Cs2 − 6 × Cl1					3.7009(5)	3.6824(1)
− 3 × Cl2					3.705(2)	3.694(1)
− 3 × Cl1					3.800(2)	3.775(2)
[Cs2−Cl]$_{avr}$					3.7267	3.70845
Cd − 6 × Br	2.8004(9)	2.7968(1)	2.7782(8)	2.7951(1)		
Cd1 − 6 × Cl1					2.600(2)	2.589(1)
Cd2 − 3 × Cl1					2.584(2)	2.576(1)
− 3 × Cl2					2.639(2)	2.626(2)
[Cd2−Cl]$_{avr}$					2.6115	2.601
Cd−Cd	3.360(1)	3.3822(1)	3.358(1)	3.3802(1)		
Cd2 − Cd2					3.327(2)	3.295(2)

Table 4
Refined compositions of CsCdBr$_3$ (**CCB**), CsCdBr$_3$:Bi (**CCB:Bi**), and CsCdCl$_3$:Bi (**CCC:Bi**) crystals according to the X-ray diffraction (**D**) and X-ray synchrotron radiation (**S**) data ($\square$ - vacancies).

Sample	D	Sample	S
CCB(D)	CsCdBr$_{2.976(42)}$	**CCB(S)**	CsCdBr$_3$
CCB:Bi(D)	(Cs$_{0.990(1)}\square_{0.010}$)(Cd$_{0.991(2)}Bi^{3+}_{0.009}$)	**CCB:Bi(S)**	(Cs$_{0.976(10)}\square_{0.024}$)(Cd$_{0.967(47)}Bi^{3+}_{0.033}$)
	(Br$_{2.970(30)}\square_{0.030}$)		Br$_3$
CCC:Bi(D)	(Cs1$_{0.989(1)}\square_{0.011}$)(Cs2)	**CCC:Bi(S)**	(Cs1$_{0.9948(2)}\square_{0.0052}$)(Cs2$_{0.9985(2)}\square_{0.0015}$)
	(Cd1$_{0.995(2)}$Bi$^{3+}_{0.005}$)		(Cd1$_{0.9873(7)}$Bi$^{3+}_{0.0127}$)
	(Cd2$_{0.996(2)}$Bi$^{3+}_{0.004}$)Cl$_6$ ≡		(Cd2$_{0.9972(43)}$Bi$^{3+}_{0.0028}$)Cl$_6$≡
	(Cs$_{0.995(2)}\square_{0.005}$)(Cd$_{0.996(2)}Bi^{3+}_{0.004}$)Cl$_3$		(Cs$_{0.9966(2)}\square_{0.0034}$)(Cd$_{0.9923(25)}Bi^{3+}_{0.0077}$)Cl$_3$

Fig. 4. The a (a) and c (b) unit cell parameters of the un-doped and Bi-doped CsCdX$_3$ crystals (X = Cl, Br) according to our and literary [20,21] data.
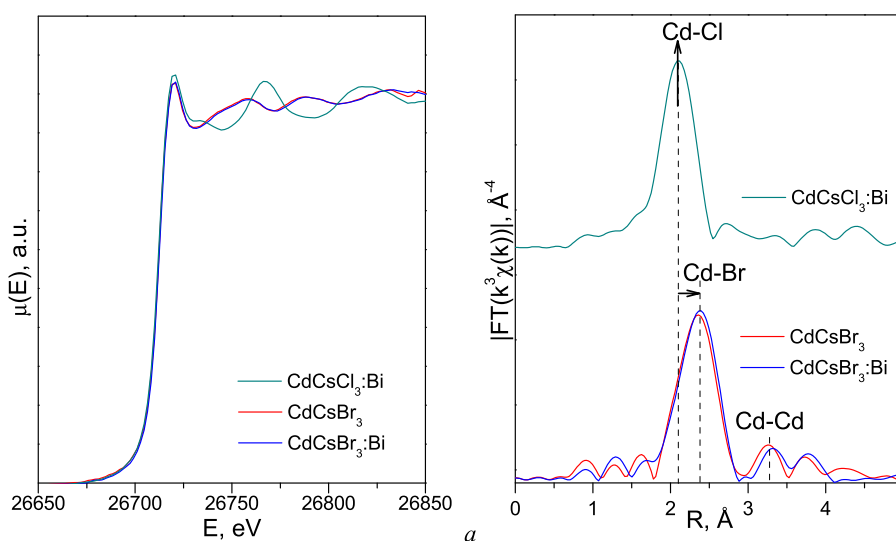
Fig. 5. The XANES spectra (*a*) and EXAFS Fourier transform curves (*b*) measured at the Cd K-edge for the CsCdBr$_3$, CsCdBr$_3$:Bi, and CsCdCl$_3$:Bi samples.

corresponding coordination numbers by relative number of atoms in each type of coordination.

In the CsCdCl$_3$ structure, Cd atoms are located in two nonequivalent, Cd1 and Cd2, sites coordinated by six Cl atoms with equal Cd1−6Cl1 and two different Cd2−(3Cl1 + 3Cl2) interatomic distances, respectively (Fig. 3, Table 3). To model the environment of each Cd atom in the CsCdCl$_3$:Bi structure, a model with three, Cd1−Cl1, Cd2−Cl1, and Cd2−Cl2, scattering paths was used (Table 5).

The EXAFS fitting procedure at the Cd K-edge for the CsCdCl$_3$:Bi sample (Fig. 5*b*, Table 5) results in the significantly increased Cd2−Cl2 interatomic distance ($d_{EXAFS} = 2.72$ Å) compared with the structural data for the CsCdCl$_3$ [21]. This means that there is an additional electron density at a distance of ~2.7−2.8 Å from the Cd atom. It cannot be caused by a presence of Bi atoms at an above-mentioned distance from the Cd ones, since Bi and Cd are not directly coordinated by each other, i.e. they are always separated by the vertex of polyhedra containing Cl atoms. At the same time, the relatively small values of the Debye factors (σ^2) obtained for Cl atoms (Table 5) indicate that the increased interatomic distance cannot be explained by a structural disorder or a presence of additional physically-nonequivalent Cd−Cl distance. Within the framework of this model, the Cd2−Cl2 distance has changed. However, if a presence of Bi atoms at the Cd site or near it is assumed, the Cl1 atom, which enters the polyhedra of both Cd atoms at the same time, is most likely to be shifted.

Thus, the EXAFS Fourier transform curves measured at the Cd K-edge confirm a distortion of the Cd coordination polyhedron when

introducing Bi into the CsCdCl$_3$ structure, it being impossible to distinguish a presence of Bi atoms at the Cd site or near it. However, since the interatomic distance Cd−Bi ~1.6 Å is physically impossible without a presence of vacancies in the Cd site, which were not observed, the Bi and Cd atoms are located in different polyhedra, having a common vertex, but with the similar environment.

The EXAFS Fourier transform curves measured at the Cd K-edge for the CsCdBr$_3$ and CsCdBr$_3$:Bi samples differ slightly: the intensities and positions for peaks of the first coordination sphere are identical (Fig. 5*b*). However, for the second coordination sphere with a maximum at 3.3 Å occupied by the Cd atoms, a simultaneous increase in the Debye factor and a small (within the error of ±1) increase in the coordination number is observed for the CsCdBr$_3$:Bi sample. It may be caused by substitution of Cd atoms for the heavier Bi ones (Bi$^{\bullet}_{Cd}$) and the associated structural disorder.

Such conclusions do not contradict the structural data obtained.

3.3. Luminescent properties

The PL spectra for the CsCdBr$_3$:Bi crystal were measured at room temperature (Fig. 6*a*) and at $T = 77$ K (Fig. 6*b*). The PL band becomes narrower with decreasing temperature (Fig. 6*b*) and its maximum is shifted to the long-wave region of the spectrum (λ ~ 1078 nm at $T = 77$ K, λ ~ 1056 nm at $T = 300$ K).

The CsCdCl$_3$:Bi exhibited PL in the near-IR spectral range having one peak at 980 nm at $T = 300$ K and at 1032 nm at $T = 77$ K when excited by light irradiation having a wavelength within the absorption bands in the visible range. Compared with the CsCdCl$_3$:Bi [19], the PL band in the spectrum measured for the CsCdBr$_3$:Bi is slightly shifted to the long-wavelength region (Fig. 6).

The PL spectra measured for the TlCdCl$_3$:Bi and TlCdI$_3$:Bi single-crystal samples excited by light having different wavelengths are given in Ref. [8]. In addition, PL bands were correlated with point defects revealed by X-ray diffraction and X-ray absorption spectroscopy. One broad PL band with a maximum at 1175 nm and two PL bands having peaks at 1025 and 1253 nm were detected for the TlCdI$_3$:Bi and TlCdCl$_3$:Bi samples, respectively [8]. The bands around λ ~1000 nm correspond to the emission of the Bi$^+$ cation (Bi$_{Tl}$)$^{\times}$. The band around λ ~1253 nm is associated with the interstitial Bi$^+$ cations (Bi$^{\bullet}_i$), the broad intense PL band with a maximum at λ ~ 1175 nm being probably due to a high concentration of interstitial Bi atoms (Bi$^{\bullet}_i$) in the TlCdI$_3$:Bi (Table 1).

Table 5
Structural parameters of the Cd local environment, obtained from the modeling of EXAFS Fourier transforms from the CsCdBr$_3$, CsCdBr$_3$:Bi, and CsCdCl$_3$:Bi samples (*N*, number of atoms; d_{EXAFS}, interatomic distance; σ^2, the Debye factor; R$_f$, the quadratic discrepancy).

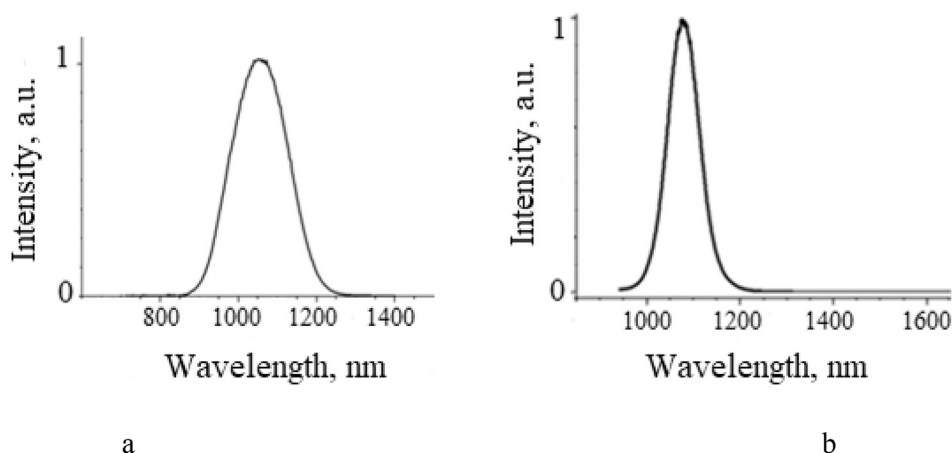| Sample	Scattering path	N	d_{EXAFS}, Å	σ^2, Å^2	R$_f$, %
CsCdBr$_3$	Cd−Br	6.0	2.73	0.0091	2.1
	Cd−Cd	1.8	3.38	0.0078	
CsCdBr$_3$:Bi	Cd−Br	6.0	2.74	0.0094	0.8
	Cd−Cd	2.3	3.36	0.0119	
CsCdCl$_3$:Bi	Cd1−Cl1	2	2.60	0.0040	1.4
	Cd2−Cl1	2	2.56	0.0022	
	Cd2−Cl2	2	2.72	0.0019	

Fig. 6. Photoluminescence spectra measured for the CsCdBr₃:Bi at $T = 300$ K (excitation wavelength, 630 nm) (a) and at $T = 77$ K (excitation wavelength, 635 nm) (b).

The temporal decay curves corresponding to a monitoring peak wavelength emission (around 1000 nm) for the Bi-doped CsCdCl₃ and CsCdBr₃ crystals excited at a wavelength of 620 nm are given in Fig. 7.

All decay curves measured were fitted to a single exponential function with characteristic times of 540 μs for the CsCdCl₃:Bi crystal and 260 μs for the CsCdBr₃:Bi crystal. It shows that the active Bi cations responsible for the IR luminescence occupy only one site (Table 1).

The PL decay from the TlCdCl₃:Bi samples after photoexcitation with a pulsed light source was studied in Ref. [8]. The characteristic lifetimes were 150 μs and 170 μs. It was assumed that an appearance of IR PL bands in the TlCdCl₃:Bi is apparently due to optical transitions between energy levels of the Bi⁺ cation located in a crystalline environment (field), similar to the KMgCl₃:Bi crystals, which also possess long-lived luminescence (Table 1) [1].

4. Summary

The firstly-performed study of the Bi-doped CsCdBr₃ and CsCdCl₃ crystals by X-ray structural analysis and X-ray absorption spectroscopy with the subsequent crystallochemical analysis of the results obtained allows us to establish the crystal real compositions, which can be described in general terms as $(Cs_{0.990(1)}\square_{0.010})(Cd_{0.991(2)}Bi^{3+}_{0.009})Br_3$ and $(Cs_{0.995(2)}\square_{0.005})(Cd_{0.996(2)}Bi^{3+}_{0.004})Cl_3$, respectively, with vacancies in the Cs site (V_{Cs}') and partial substitution of Cd^{2+} ions for the Bi^{3+} ($Bi^{\bullet}_{Cd}$) ones. The refined crystal compositions are confirmed by the EXAFS/XANES results and the PL band in the near-IR

spectral range with a maximum at $\lambda = 1078$ nm ($T = 77$ K) and $\lambda = 1056$ nm ($T = 300$ K) for the CsCdBr₃:Bi and at $\lambda = 980$ nm ($T = 300$ K) and $\lambda = 1032$ nm ($T = 77$ K) for the CsCdCl₃:Bi, which is found to be associated with the $Bi^{\bullet}_{Cd}$ point defects (Table 1).

The assumed presence of Bi¹⁺ ions in the structures of CsCdBr₃ and CsCdCl₃ crystals, similar to the TlCdCl₃:Bi¹⁺ and TlCdI₃:Bi¹⁺ ones studied by our scientific group earlier [8], is not confirmed, which is consistent with the theory of isomorphic mixing of components [24]. A difference in the structural behavior of Bi ions in the TlCdI₃:Bi (the Bi¹⁺ ions occupy interstitials, $Bi^{\bullet}_i$) and TlCdCl₃:Bi (the Bi¹⁺ ions occupy interstitial ($Bi^{\bullet}_i$) and Tl¹⁺ ($Bi^{\times}_{Tl}$) sites) [8] and in the CsCdCl₃:Bi and CsCdBr₃:Bi (the Bi³⁺ ions substitute for the Cd²⁺ ions, $Bi^{\bullet}_{Cd}$; it is found by X-ray diffraction and confirmed by EXAFS/XANES) crystals is due to the chemical similarity of Tl¹⁺ ($r^{XII}_{Tl} = 1.70$ Å, $\chi_{Tl} = 1.5$ a.u.) and Bi¹⁺ ($r^{XII}_{Bi} = 1.903$ Å, $\chi_{Bi1+} = 1.4$ a.u.) ions, in contrast to the Cs¹⁺ and Bi¹⁺ ions. However, a large difference in the Tl¹⁺ and Bi¹⁺ ionic sizes ($\Delta r = 0.203$ Å), despite a small difference between the electronegativity values ($\Delta \chi = 0.1$ a.u.), severely limits a substitution of Tl¹⁺ ions for the Bi¹⁺ ones in TlCdX_3:Bi structures and results in the location of a significant number of Bi¹⁺ ions in the vicinity of the Tl¹⁺ site ($Bi^{\bullet}_i$), which is possible only in combination with vacancies in this site (V_{Tl}'). For the TlCdX_3:Bi structures [8], the rules of assistance (the $Bi^{\bullet}_i$ content is higher in the TlCdI₃:Bi compared to the TlCdCl₃:Bi; $R_I > R_{Cl}$) and polarity (the Bi¹⁺ ions do not replace the Ti¹⁺ ones in TlCdX_3:Bi structures in the quantity defined by the XRD; rBi $> r$Tl) are also fulfilled. It should be noted that the rules of isomorphic mixing may be useful in the analysis of systems in which a presence of Bi¹⁺ ions
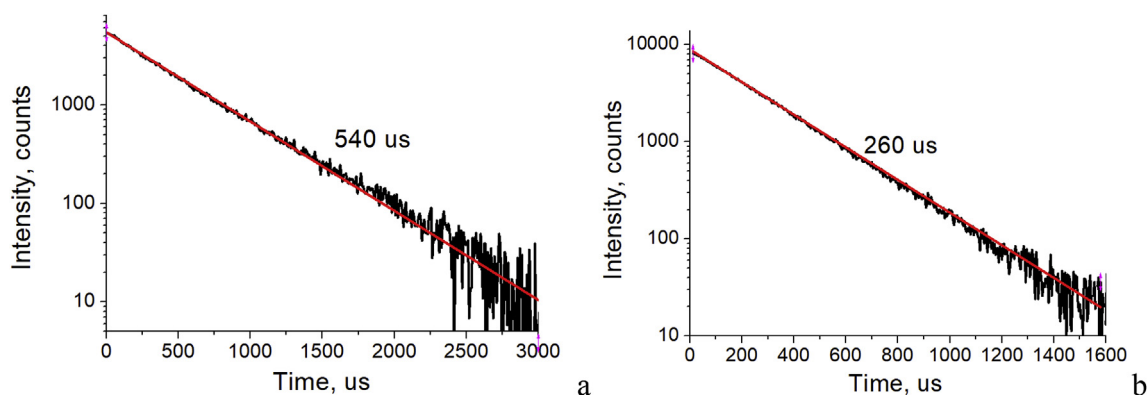

Fig. 7. Photoluminescence decay curves for the CsCdCl₃:Bi (a) and CsCdBr₃:Bi (b) crystals excited at 620 nm.

is assumed. The formal charge of Bi ions and their location in the crystal lattice can be determined by structural analysis combined with the X-ray absorption spectroscopy (EXAFS/XANES), followed by the determination of correlation between the data obtained and luminescent properties, as evidenced by the results of present work.

Photoluminescent properties of known complex halides (Table 1) indicate different PL decay times (the smallest and the highest values were found for the $TlCdI_3:Bi^{1+}$ and $CsCdCl_3:Bi^{3+}$, respectively), which results in a wide range of their possible application for both devices with a high-speed optical response and long afterglow phosphors.

Acknowlegements

References

[1] A.N. Romanov, A.A. Veber, Z.T. Fattakhova, O.V. Usovich, E.V. Haula, L.A. Trusov, P.E. Kazin, V.N. Korchak, V.B. Tsvetkov, V.B. Sulimov, Subvalent bismuth monocation Bi^+ photoluminescence in ternary halide crystals $KAlCl_4$ and $KMgCl_3$, J. Lumin. 134 (2013) 180—183.

[2] C. Li, Z. Song, J. Qiu, Z. Yang, X. Yu, D. Zhou, Z. Yin, R. Wang, Y. Xu, Y. Cao, Broadband yellow—white and near infrared luminescence from Bi-doped $Ba_{10}(PO_4)_6Cl_2$ prepared in reductive atmosphere, J. Lumin. 132 (7) (2012) 1807—1811.

[3] L. Su, H. Zhao, H. Li, L. Zheng, G. Ren, J. Xu, W. Ryba-Romanowski, R. Lisiecki, P. Solarz, Near-infrared ultrabroadband luminescence spectra properties of subvalent bismuth in CsI halide crystals, Opt. Lett. 36 (23) (2011) 4551—4553.

[4] A.G. Okhrimchuk, L.N. Butvina, E.M. Dianov, N.V. Lichkova, V.N. Zagorodnev, K.N. Boldyrev, Near-infrared luminescence of $RbPb_2Cl_5$:Bi crystals, Opt. Lett. 33 (19) (2008) 2182—2184.

[5] X.G. Meng, J.R. Qiu, M.Y. Peng, D.P. Chen, Q.Z. Zhao, X.W. Jiang, C.S. Zhu, Near infrared broadband emission of bismuth-doped aluminophosphate glass, Optic Express 13 (5) (2005) 1628—1634.

[6] A.N. Romanov, A.A. Veber, D.N. Vtyurina, Z.T. Fattakhova, E.V. Haula, D.P. Shashkin, V.B. Sulimov, V.B. Tsvetkov, V.N. Korchak, Near infrared photoluminescence of the univalent bismuth impurity center in leucite and pollucite crystal hosts, J. Mater. Chem. C 3 (15) (2015) 3592—3598.

[7] A.A. Veber, A.N. Romanov, O.V. Usovich, Z.T. Fattakhova, E.V. Haula, V.N. Korchak, L.A. Trusov, P.E. Kazin, V.B. Sulimov, V.B. Tsvetkov, Optical properties of the Bi^+ center in $KAlCl_4$, J. Lumin. 151 (2014) 247—255.

[8] D.N. Vtyurina, P.A. Eistrikh-Geller, G.M. Kuz'micheva, V.B. Rybakov, E.V. Khramov, I.A. Kaurova, D. Yu. Chernyshov, V.N. Korchak, Influence of monovalent Bi^+ doping on real composition, point defects, and photoluminescence in $TlCdCl_3$ and $TlCdI_3$ single crystals, Sci. China Mater. 60 (12)

[9] A.N. Romanov, F.V. Grigoriev, V.B. Sulimov, Estimation of Bi^+ monocation crystal ionic radius by quantum chemical simulation, Comput. Theor. Chem. 1017 (2013) 159—161.

[10] A. Wolfert, G. Blasse, Luminescence of s^2 ions in $CsCdBr_3$ and $CsMgCl_3$, J. Solid State Chem. 55 (3) (1984) 344—352.

[11] L.J. Farrugia, WinGX and ORTEP for windows: an update, J. Appl. Crystallogr. 45 (4) (2012) 849—854.

[12] V. Dyadkin, P. Pattison, V. Dmitriev, D. Chernyshov, A new multipurpose diffractometer PILATUS@SNBL, J. Synchrotron Radiat. 23 (3) (2016) 825—829.

[13] Agilent, CrysAlis PRO. Version 1.171.37.35, Agilent Technologies Ltd, Yarnton, Oxfordshire, England, 2014.

[14] G.M. Sheldrick, SHELXT—Integrated space-group and crystal-structure determination, Acta Crystallogr. A: Found. Adv. 71 (1) (2015) 3—8.

[15] A.C.T. North, D.T. Phillips, F.S. Mathews, A semi-empirical method of absorption correction, Acta Crystallogr. - Sect. A Cryst. Phys. Diffr. Theor. Gen. Crystallogr. 24 (3) (1968) 351—359.

[16] G.M. Kuz'micheva, I.A. Kaurova, E.A. Zagorul'ko, N.B. Bolotina, V.B. Rybakov, A.A. Brykovskiy, E.V. Zharikov, D.A. Lis, K.A. Subbotin, Structural perfection of $(Na_{0.5}Gd_{0.5})MoO_4$:Yb laser crystals, Acta Mater. 87 (2015) 25—33.

[17] N.N. Trofimova, A.A. Veligzhanin, V.Y. Murzin, A.A. Chernyshov, E.V. Khramov, V.N. Zabluda, I.S. Edel'man, Yu. L. Slovokhotov, Y.V. Zubavichus, Structural diagnostics of functional nanomaterials with the use of X-ray synchrotron radiation, Nanotechnol. Russia 8 (5—6) (2013) 396—401.

[18] B. Ravel, M. Newville, ATHENA, ARTEMIS, HEPHAESTUS: data analysis for X-ray absorption spectroscopy using IFEFFIT, J. Synchrotron Radiat. 12 (4) (2005) 537—541.

[19] A.N. Romanov, A.A. Veber, Z.T. Fattakhova, D.N. Vtyurina, M.S. Kouznetsov, K.S. Zaramenskikh, I.S. Lisitsky, V.N. Korchak, V.B. Tsvetkov, V.B. Sulimov, Spectral properties and NIR photoluminescence of Bi^+ impurity in $CsCdCl_3$ ternary chloride, J. Lumin. 149 (2014) 292—296.

[20] R.D. Shannon, Revised effective ionic radii and systematic studies of interatomic distances in halides and chalcogenides, Acta Crystallogr. - Sect. A Cryst. Phys. Diffr. Theor. Gen. Crystallogr. 32 (5) (1976) 751—767.

[21] S. Siegel, E. Gebert, The structures of hexagonal $CsCdCl_3$ and tetragonal Cs_2CdCl_4, Acta Crystallogr. 17 (6) (1964), 790-790.

[22] G.L. McPherson, A.M. McPherson, J.L. Atwood, Structures of $CsMgBr_3$, $CsCdBr_3$ and $CsMgI_3$ – diamagnetic linear chain lattices, J. Phys. Chem. Solids 41 (5) (1980) 495—499.

[23] K.S. Aleksandrov, V.V. Beznosikov, Hierarchies of perovskite-like crystals, Phys. Solid State 39 (5) (1997) 695—715.

[24] V.S. Urusov, Theory of Isomorphic Mixing Ability, Nauka, Moscow, 1977 (in Russian).

[25] J. Neukum, N. Bodenschatz, J. Heber, Spectroscopy and upconversion of $CsCdBr_3:Pr^{3+}$, Phys. Rev. B 50 (6) (1994) 3536.

[26] B.Z. Malkin, A.I. Iskhakova, V.F. Tarasov, G.S. Shakurov, J. Heber, M. Altwein, Submillimeter EPR spectroscopy of lanthanide compounds: pair centers of Ho^{3+} in $CsCdBr_3$, J. Alloy. Comp. 275 (1998) 209—213.

[27] V.F. Tarasov, G.S. Shakurov, B.Z. Malkin, A.I. Iskhakova, J. Heber, M. Altwein, Submillimeter electron-nuclear excitation spectra in $CsCdBr_3$:Ln^{3+} (Ln = Tm, Ho) crystals, J. Exp. Theor. Phys. Lett. 65 (7) (1997) 559—565.

[28] V. Mehta, O. Guillot-Noël, D. Simons, D. Gourier, P. Goldner, F. Pellé, EPR Identification of coupled Yb^{3+} ion pairs in optically bistable compound $CsCdBr_3$:Yb, J. Alloy. Comp. 323 (2001) 308—311.